First-principles analysis of photocurrent in graphene *PN* junctions

Jingzhe Chen,* Yibin Hu, and Hong Guo
Centre for the Physics of Materials and Department of Physics, McGill University, Montreal, PQ, Canada H3A 2T8
(Received 4 November 2011; revised manuscript received 20 February 2012; published 23 April 2012)

We report on a first-principles investigation of photocurrent generation by graphene *PN* junctions. The junctions are formed by either chemically doping with nitrogen and boron atoms, or by controlling gate voltages. The nonequilibrium Green's function formalism combined with density functional theory is applied to calculate the photoresponse function. The graphene *PN* junctions show a broadband photoresponse including the terahertz range. The dependence of the response on the angle between the light polarization vector and the *PN* interface is determined. Its variation against photon energy $E_{\rm ph}$ is calculated in the visible range. The essential properties of chemically doped and gate-controlled *PN* junctions are similar, but the former shows fingerprints of dopant distribution.

DOI: 10.1103/PhysRevB.85.155441 PACS number(s): 73.20.−r, 73.40.−c, 73.50.Pz, 73.63.−b

I. INTRODUCTION

The extraordinary electronic and optical properties of graphene make it a promising material for novel applications in photonics and optoelectronics.[1] Experimental investigations have discovered several very interesting behaviors of graphene. Some are quite unique, such as the universal optical conductance, high transparency,[2] and broadband nonlinear photoluminescence.[3] Possible applications include transparent electrodes, photovoltaic cells, and touch screens.[4,5] One of the most interesting applications is the graphene photodetector. The gapless nature of graphene implies that there may always be an electron-hole pair in resonance with any excitation, allowing a broad operational wavelength ranging from 300 nm to 6 μm which can overcome the long-wavelength limit of conventional semiconductors.[6,7] Once excited, due to the high carrier mobility of graphene, hot electrons can transfer energy to the entire system in very short time scales ($\sim$1 ps),[8,9] and a 10 Gbit s^{-1} optical data link for error-free detection of an optical data stream has been reported.[10,11] These results demonstrate a great potential of graphene to be an advanced material for light sensors and high-speed communications.

A dipole potential is necessary for the photovoltaic (PV) process that produces a net dc electric current. For a graphene system, it can be achieved by either tuning a gate voltage locally or chemically doping acceptor and donor atoms at different regions. Many interesting predictions or experiments are reported in these graphene *PN* junctions. For example, Veselago effects or Fabry-Pérot oscillations can happen in different situations without light;[12] with light, photocurrent has been produced in both gate-controlled and chemically doped junctions.[13–15] The chemically doped graphene *PN* junction is more common in experimental studies; the gate-controlled junction is more difficult to fabricate since it requires a more precise setup of the device structure and light illumination. For the chemical junctions, the doping level lies within hundreds of millivolts, which corresponds to terahertz or far-infrared frequencies; on the other hand, the gate-controlled junction is able to reach the higher-frequency regime.

The photoresponse behavior of graphene *PN* junctions is very important and warrants systematical theoretical investigations. Recently, Refs. 16 and 17 reported theoretical analysis of gate-controlled graphene *PN* junctions by solving a model Hamiltonian and determining photoresponse within a semiclassical transport model. To the best of our knowledge, the photoresponse of graphene *PN* junctions has not been investigated from an atomistic first-principles point of view. It is the purpose of this work to fill this gap, and we investigate the photoresponse function for both chemical and gate-controlled systems. In particular, photoresponse in a broad frequency range including the terahertz range is investigated. Such a broadband photoresponse is difficult to achieve with conventional semiconductors. The dependence of photoresponse on the angle between the direction of light polarization and the *PN* interface is determined. This dependence is found to be well consistent with the previous theoretical result.[16] We also determined the dependence of photoresponse on photon energy $E_{\rm ph}$ in the range of $E_{\rm ph}$–U, where U is the potential decline in the depletion region of the *PN* junction. In the solar visible range, for $E_{\rm ph} < U$ the photoresponse is almost linear, in agreement with that found in Ref. 17, and it tends to saturate when $E_{\rm ph}$ exceeds U. Signatures of dopant distribution can be found in the photoresponse function of the chemical junctions. By investigating both chemical doping and gate control, the PV properties of graphene *PN* junctions are compared and a comprehensive understanding is achieved. Finally, our atomistic approach provides a benchmark result for first-principles optoelectronic studies of the graphene system.

The rest of the paper is organized as follows. In the next section, the calculation method is presented. Sections III and IV present results for the chemically doped and gate-controlled junctions, respectively. The last section is reserved a for short discussion and a summary.

II. METHOD

A two-probe graphene PV device consists of a scattering region sandwiched by the left and right graphene electrodes. Figure 1(a) plots such a two-probe PV system showing a chemically doped graphene *PN* junction. Here, a *PN* junction is formed by doping nitrogen (N, blue) on the left of the junction and boron (B, pink) on the right. The scattering region of the device consists of the *PN* junction and many layers of (doped) graphene on the left and right. Far from the *PN* junction, the scattering region connects to the left and right electrodes: the electrode atoms are shown in the

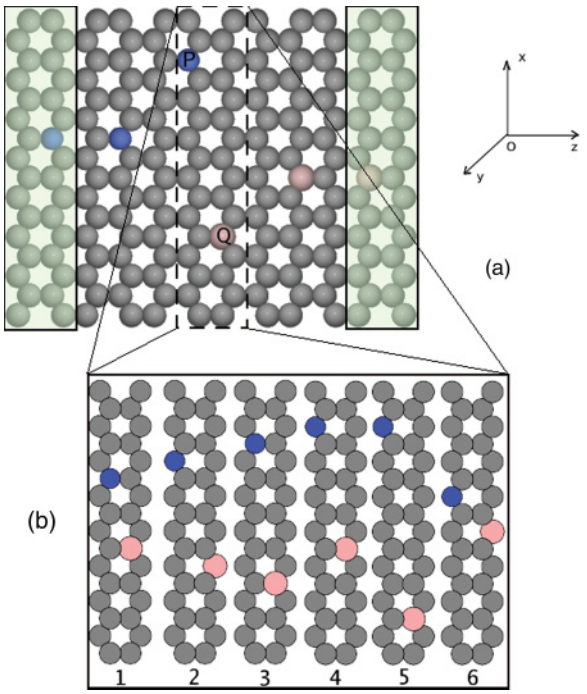

FIG. 1. (Color online) (a) Schematic atomic structure of the PN junction. The system is a graphene sheet doped with N (blue) atoms on the left side and B (pink) atoms on the right. The regions in shadow are part of the electrodes which extend periodically to $z \pm \infty$. dc current flows from the left to the right (along the z axis) or vice versa. In the first-principles calculations, the device is treated as periodic in the x and y directions. In the y direction, a large vacuum region is included in the calculation supercell that effectively isolates interactions between the graphene sheet and its periodic images. **P** and **Q** represent positions of dopant atoms at the interface. (b) The six interface patterns of the chemical junction analyzed in this paper.

shadowed boxes. The electrodes extend to electron reservoirs at $z = \pm\infty$ where photocurrent is collected. In the analysis, the scattering region should be large enough (12 atomic layers in our calculations) so that the electronic structure of the electrodes is not affected by the charge transfer at the PN junction in the middle of the structure.

Because current flow is intrinsically a nonequilibrium transport problem, our calculation is based on carrying out real-space density functional theory (DFT) calculation within the Keldysh nonequilibrium Green's function (NEGF) formalism.[18] Very briefly, in the NEGF-DFT formalism, DFT is used to self-consistently calculate the electronic structure and Hamiltonian of the device; the NEGF is used to determined the quantum statistical information that is needed to populate the electronic structure and calculate the density matrix; real-space numerical methods are used to handle the transport and electrostatic boundary conditions at the interface between the electrodes and the device scattering region. Since the NEGF-DFT method has been well documented, we refer interested readers to the original literature for more details.[18] In this work, a GPAW implementation[19] of the NEGF-DFT is used for the calculations.

Our interest in this work is to analyze the photoresponse of the PV device. A linear polarized light is shined on the scattering region and not the electrodes. This is reasonable because a very long graphene nanoribbon (>1000 nm) can be fabricated experimentally[20] and the electrodes can be covered by optically nontransparent materials. To obtain the corresponding photocurrent, we first calculate the Hamiltonian $\hat{H}_0$ of the two-probe PV device [e.g., Fig. 1(a)] without light, using the NEGF-DFT self-consistent method.[18,19] Here, the exchange correlation is treated with the Perdew-Burke-Ernzerhof (PBE) functional[21] and a (4,1) k-mesh is applied the in x-y plane for k-sampling. A single zeta polarized (SZP) atomic orbital basis set is used to expand all the physical quantities. For graphene, the SZP basis is sufficient for obtaining accurate results.

After $\hat{H}_0$ is self-consistently calculated, electron-photon interaction is added to it as a perturbation for the subsequent analysis of photocurrent. This way, the total Hamiltonian of the electron-photon system is

$$\hat{H} = \hat{H}_0 + \frac{e}{m_0}\mathbf{A}\cdot\hat{\mathbf{p}}, \tag{1}$$

where A is the polarization vector of the light. Assuming the electromagnetic field of a photon is a single-mode monochromatic plane wave, and also assuming the susceptibility and dielectric constants to be homogeneous, we have[22]

$$\mathbf{A}(t) = \hat{a}\left(\frac{\hbar\sqrt{\tilde{\mu_r}\tilde{\epsilon_r}}}{2N\omega\tilde{\epsilon}c}I_\omega\right)^{1/2}(be^{-i\omega t} + b^\dagger e^{i\omega t}), \tag{2}$$

where $\tilde{\mu_r}$, $\tilde{\epsilon_r}$, and $\tilde{\epsilon}$ are the relative susceptibility, relative dielectric constant, and absolute dielectric constant, respectively. $\hat{a}$ represents polarization of the field, and I_ω is the photon flux defined as the number of photons per unit time per unit area,

$$I_\omega \equiv \frac{Nc}{V\sqrt{\tilde{\mu_r}\tilde{\epsilon_r}}}. \tag{3}$$

The first-order electron-photon Keldysh self-energies are[22,23]

$$\Sigma^{\gtrless}_{lm}(E) = \sum_{pq} M_{lp}M_{qm}\left[NG^{0\gtrless}_{pq}(E \pm \hbar\omega) + (N+1)G^{0\gtrless}_{pq}(E \mp \hbar\omega)\right], \tag{4}$$

where $M_{lm} \equiv \frac{e}{m_0}(\frac{\hbar\sqrt{\tilde{\mu_r}\tilde{\epsilon_r}}}{2N\omega\tilde{\epsilon}c}I_\omega)^{1/2}\langle l|p_z|m\rangle$, assuming z to be the light-polarization direction. The Keldysh Green's functions are written as

$$G^< = G^{0r}(i\Gamma_L f_L + i\Gamma_R f_R + \Sigma^<_{\rm ph})G^{0a}\,, \tag{5}$$

$$G^> = G^{0r}[i\Gamma_L(1-f_L) + i\Gamma_R(1-f_R) + \Sigma^>_{\rm ph}]G^{0a}, \tag{6}$$

where Γ represents the coupling of the device scattering region to the electrodes, namely the linewidth function of the electrodes. G^{0r} and G^{0a} are the retarded and advanced Green's functions (without photons), respectively. In Eq. (4), $G^{0\gtrless}$ is calculated by Eqs. (5) and (6) without the electron-photon interaction.

With the ground-state Hamiltonian $\hat{H}_0$ of the two-probe PV device, quantities Γ, G^{0r}, G^{0a}, and $G^{0\gtrless}$ can be calculated.[18] Afterward, $\Sigma^{\gtrless}$ is calculated via Eq. (4), which can then be put into Eqs. (5) and (6) to determine the Keldysh Green's function $G^{\gtrless}$.

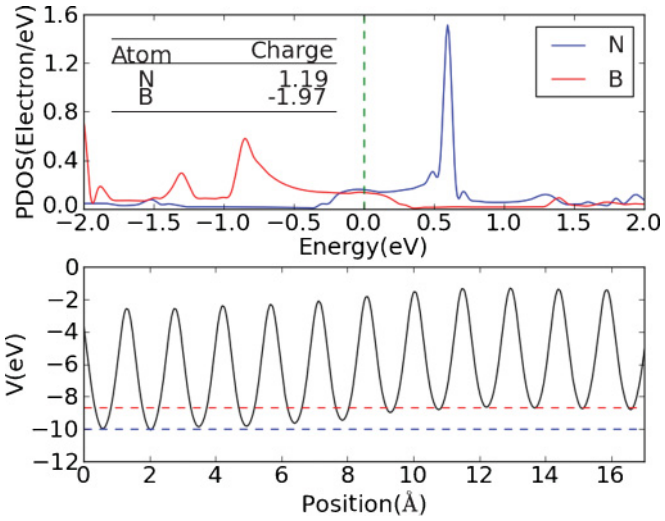

FIG. 2. (Color online) Upper panel: the PDOS of N and B atoms. There is a donor peak of N around 0.6 eV (blue peak) and an acceptor peak of B around −0.9 eV (red peak). The dashed vertical line at energy zero is the Fermi level. The result of Bader charge-transfer analysis is listed in the inset table. Lower panel: averaged effective potential profile along the transport direction. Blue dashed line represents the level in the left electrode and red dashed line is for the right.

Finally, following Ref. 24, the linear phase-coherent photocurrent is calculated with the following formula:

$$I_{\rm ph} = \frac{ie}{2\hbar}\int \frac{d\epsilon}{2\pi}{\rm Tr}\{[\Gamma^L(\epsilon)-\Gamma^R(\epsilon)]G^<(\epsilon)+[f_L(\epsilon)\Gamma^L(\epsilon) - f_R(\epsilon)\Gamma^R(\epsilon)][G^r(\epsilon)-G^a(\epsilon)]\}. \quad (7)$$

Since the photon field is taken as a perturbation to $\hat{H}_0$, the photocurrent obtained in this way is in the small intensity regime and nonlinear optical effects are not considered in this work.

III. CHEMICALLY DOPED JUNCTIONS

For the chemically doped graphene PN junction, the schematic atomic structure is shown in Fig. 1(a), where a heterojunction is formed by doping the two sides with nitrogen or boron atoms, respectively. We investigated six junctions with different dopant configurations [Fig. 1(b)]. For these junctions, while it is more realistic to use metal leads far away from the PN junction to collect current and connect the PN junction to the outside world, to reduce the computational demand we extended the doped graphene to $z = \pm\infty$ to act as device leads. This is acceptable because photocurrent is generated in the PN junction where the dipole potential is located.

To be specific, let us consider a particular configuration [the sixth pattern in Fig. 1(b)]. Figure 2 plots the calculated ground-state properties without photons. The partial density of states (PDOS) in the upper panel of Fig. 2 shows two characteristic peaks which are contributed by the donor (N) and acceptor (B) atoms just above and below the Fermi level (dashed vertical line). As a donor, the N atoms give electrons to the graphene, which is indicated by its PDOS peak being above the Fermi level (blue peak near 0.6 eV). Similarly, the B atoms accept electrons, and the graphene's PDOS peak is located below the Fermi level (red peak near −0.9 eV). On the other hand, a Bader charge analysis shows that the N atom actually gains some charge, $1.19e$ on average, and the B atom loses about $1.97e$ (see the table in the upper panel of Fig. 2)—these are in agreement with previous literature.[25] Hence the Bader charge analysis appears to contradict N and B atoms being donors and acceptors. A further detailed analysis showed that the carbon atoms in the N side of the junction lose electrons in total but gain electrons in their p_y orbital, which forms conjugate π states for charge carriers that contribute to transport. On the B side of the junction, the carbon atoms lose π electrons. In other words, the N atoms lose some high-energy level charges as donors while attracting more low-energy level covalent electrons due to greater electron affinity. The situation of B atoms is analogous to that of N. This way, by separating the transport carriers (the π electrons) from the total electron number on the atoms, the Bader charge analysis is reconciled with the roles of N and B atoms being donors and acceptors.

The carbon atoms in the system, to some extent, follow the behavior of the dopants, i.e., the C atoms in the N or B side form an extra conduction or valence band, respectively. Then, an electron in the extra valence bands (contributed by (B) and [C(B)]) can absorb a photon and hop to the extra conduction bands (contributed by (N) and [C(N)]) across the Fermi level, eventually giving rise to the electron flow from the B to the N side of the PN junction. This is also reflected in the average effective potential shown in the lower panel of Fig. 2, where we observe a potential decline about ∼1.4 eV at the interface (the oscillation is due to the ionic potential). An electron-hole pair is generated after absorbing a photon. The electron flows along the potential decline and the hole in the opposite direction. A photocurrent is therefore generated in the graphene PN junction by the photovoltaic effect without external bias.

We now turn on the light and investigate the dependence of photoresponse to light polarization. Figure 3 plots the photoresponse function,

$$f \equiv \frac{I_{\rm ph}}{eF}, \quad (8)$$

versus photon energy with different polarization directions of the light. Here, F is the photon flux: in our perturbation theory, photocurrent scales with F. θ in Fig. 3 is the angle between the direction of light polarization and the y axis. The photocurrent almost vanishes completely when $\theta = 0$, i.e., when the electric field of the light vibrates along the y axis. This is because the angular momentum quantum number of such a photon is equal to 1 along the y axis, while both the valence band in the B side and the conduction band in the N side of the PN junction are in the π orbital, also having unity angular momentum quantum number along the y axis. The photon-induced hoping from the valence band to the conduction band is therefore prohibited due to the mismatch of the three angular quantum numbers. This limitation starts to be relieved when θ increases from zero and is completely removed when θ reaches $\pi/2$, at which the maximum photocurrent is reached. As a direct result of Fermi's golden rule, the photocurrent scales with $\sin^2\theta$, where θ changes from 0 to $\pi/2$ (see the inset of Fig. 3), which is in

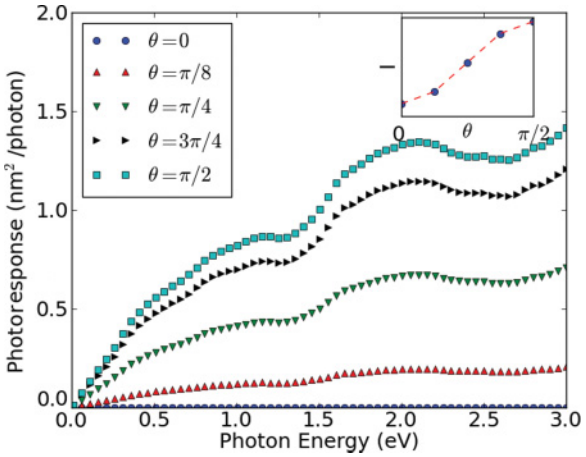

FIG. 3. (Color online) Photoresponse function with different light-polarization directions. The polarization direction changes continuously from the π orbital direction (y axis) to the transport direction (z axis). Inset: photocurrent at photon energy 2.0 eV vs different polarization angles. The red dashed line is fitting to the trigonometric function $I_{\pi/2}\sin^2\theta$.

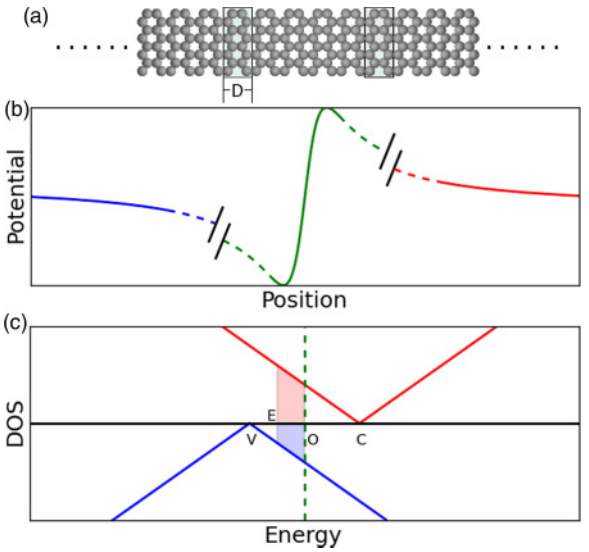

FIG. 4. (Color online) (a) Gate-controlled PN junction: it is a perfect graphene sheet with two local metal gates (shown as green shadowed boxes) on top. Coordinates are defined in the same way as in Fig. 1(a). (b) Schematic plot of a dipole potential along the transport (z axis) direction. At $z=\pm\infty$, the potential equals that of perfect graphene. Dashed lines indicate the slowly decaying potential over a long distance. (c) The DOS of the gate-controlled graphene PN junction. The region above the horizontal black line is for a positive gate voltage (right side) where the linear Dirac bands are shifted upward; the region below is for a negative gate voltage (left side). The green vertical dashed line indicates the Fermi level. Shadowed areas represent the region where electrons can be excited by photons to contribute to the photocurrent.

good agreement with the results of Ref. 16. Since the angle dependence is determined by the angular momentum of the π orbital, the gate-controlled PN junctions to be discussed below show the same trend.

Different from the discrete features predicted for carbon nanotubes,[26] the photoresponse of graphene is smooth over a broad frequency range corresponding to the continuous spectrum of the graphene material (e.g., Dirac bands near the Fermi level). In other words, there are no obvious transition features between discrete states in the f-$E_{\rm ph}$ curve. Photons with energy $E_{\rm ph}$ can excite electrons in the range $[-E_{\rm ph},0]$ to generate electron-hole pairs; these pairs can be separated in the depletion region of the PN junction and contribute to the photocurrent.

We have also investigated the role of dopant distribution by comparing the results of six samples having different dopant locations [only the positions indicated by letters P and Q in Fig. 1(a) are randomly changed]. These results will be compared with those of the gate-controlled PN junctions in the next section.

IV. GATE-CONTROLLED JUNCTION

The structure of a gate-controlled device is shown in Fig. 4(a). We imagine that a metal gate of finite width D is attached on either side of the graphene forming a transport junction. When opposite gate voltages are applied on the two gates, a potential drop is established across the junction. Far left to the left gate and far right to the right gate, the system is not affected by the gate potentials so that the two electrodes far away still have the same chemical potential, as schematically shown in the potential profile in Fig. 4(b). Without photons, there is no dc current because the electrochemical potentials of the left and right reservoirs are the same. With photons, electrons may be excited from the valence DOS [as indicated by the shadowed area in Fig. 4(c)] to the conduction DOS, and a net dc current is generated by the local electric field.

In practical calculations, gate voltages can be applied as the electrostatic boundary conditions for the Hartree potential.[27] For graphene, the potential decays very slowly due to poor screening of low dimensionality, as schematically indicated in Fig. 4(b): a very long graphene sheet between the two gates would be needed in the calculation to correctly capture the potential profile. This computation difficulty can be bypassed approximately. In our analysis, we neglect electron-hole pair splitting in the decaying region of the potential. This is well justified due to the weak local electric field. We also neglect any change (due to the gate) in the self-energy: this is similar to the wide-band approximation. Hence, the gate voltages can be simulated in the NEGF-DFT method very simply as follows. We first carry out a NEGF-DFT self-consistent analysis of homogeneous graphene, increasing the bias voltage to U, and then we reset the electrochemical potentials of both electrodes to the Fermi level of the unbiased graphene in subsequent photocurrent calculations. As a result, the junction produces photocurrent when the scattering region (between the gates) is under light illumination.

In Fig. 5, we plot the photoresponse function f [Eq. (8)] subjected to different gate-voltage differences U for the gate-controlled junction versus the photon energy $E_{\rm ph}=\hbar\omega$. When $E_{\rm ph}<U$, f increases linearly with $E_{\rm ph}$. In Refs. 16 and 17, by solving a semiclassical transport model, the photoresponse function $f=\frac{\hbar\omega I}{eS}$ under certain light intensity S is also found to be linear in photon energy, $f=\frac{\pi e^2 W\omega}{2c\beta}\propto\omega$ when $\hbar\omega\sim U$

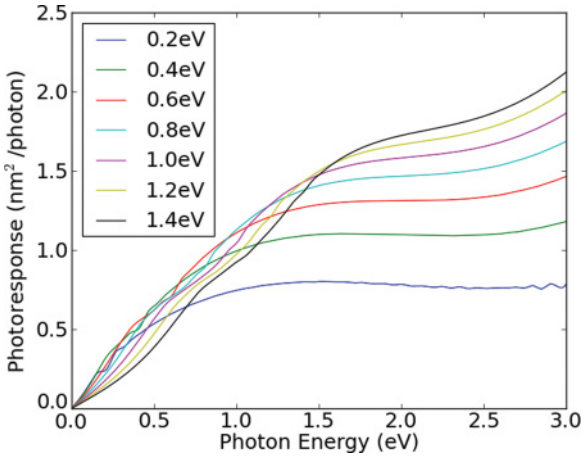

FIG. 5. (Color online) Photoresponse function of the gate-controlled graphene PN junction under different gate voltage differences U displayed in the legend. On the right of this figure (higher photon energy range), the curves are ordered from low U to high U, i.e., the lowest curve is $U = 0.2$ V and the highest curve is $U = 1.4$ V.

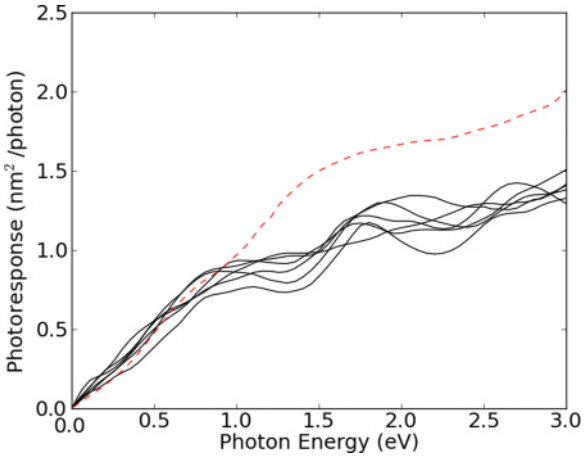

FIG. 6. (Color online) Black solid curves are the photoresponse function for junctions with different dopant configuration [interface structures shown in Fig. 1(b)]. The red dotted curve is the photoresponse of the gate-controlled PN junction having an average potential decline of 1.4 eV. The polarization angle of the incident light is set to $\theta = \pi/2$ for all cases.

(W is the width of the strip and β is the slope of the potential). Here we give a simple argument of the linear relationship when $E_{\rm ph} \sim U$—based on the intrinsic linear dispersion of graphene. As shown in Fig. 4(c), the V-shaped DOS of pristine graphene is shifted above or below the Fermi level by the gate voltage, and the distance between the two dips (labeled C and V) is the difference U between the gate voltages. A photon with energy $E_{\rm ph}$ can excite valence electrons having energies in the range $[E_{\rm ph}, 0]$ to the conduction band, i.e., the number of excited electrons $N_{\rm ex}$ is proportional to the shadowed area indicated in Fig. 4(c). The excited electrons are collected by electrodes at the edge of the scattering region where the coupling Hamiltonian can be simplified as $i\Gamma$ (Γ is a constant representing the lifetime of the electron at the edge). Photocurrent is therefore determined by two factors: $I_{\rm ph} \propto N_{\rm ex}\Gamma$. In Fig. 4(c), the red shadowed area means that the electron is excited from the right side to the left side of the junction, and the opposite is true for the blue shadowed area. The photocurrents contributed by these two areas have opposite sign, and the net current depends on their difference. Due to the linear dispersion of graphene, the difference of these two areas scales with $E_{\rm ph}$, therefore the photoresponse photocurrent induced by one photon is linear to $E_{\rm ph}$. For $E_{\rm ph} > U$, the response involves more complicate factors rather than the π bands. From the results, we conclude that it tends to saturate and appears quite flat over a broad range of $E_{\rm ph}$.[28]

A very interesting issue to explore is how a gate-controlled device compares with the chemically doped ones. To this end, we calculated six samples of chemically doped devices in which the dopant locations are different [positions indicated by letters P and Q in Fig. 1(a)]. The results of the gate-controlled device and the six chemically doped devices are shown in Fig. 6. At low energy, the photoresponses of all the devices are similar, suggesting that the response is mostly determined by the overall potential slope of the PN junction, i.e., the carbon system provides the main contribution to photocurrent. When photon energy is larger than 1 eV, the photoresponses start to differ from each other. The chemically doped junctions have some specific undulations (black curves in Fig. 6) which can be traced to dopant scattering. This is a characteristic fingerprint due to quantum interference between different electron-propagating paths. The photoresponse of the gate-controlled junction is smooth since the potential profile is relatively smooth.[29] It also has a larger response in the high-frequency regime. This is because in chemically doped junctions, the strong local fields near the dopants may not contribute to photocurrent if the donor and acceptor sit far apart from each other, and, on average, for chemical junctions the active carbon system suffers from a weaker global field across the PN junction as compared to that of the gate-controlled junctions.

V. DISCUSSION AND SUMMARY

The calculated values of the photoresponse function imply that for an ∼1-mm-wide graphene PN junction (the light is shined perpendicularly to the junction plane), at the standard solar light intensity of 0.1 W/cm^2 and a photon energy of 1 eV, the corresponding photocurrent should be on the order of nA, which is detectable experimentally. For the chemically doped graphene PN junctions with high dopant concentration, short-range disorder may trigger charge localization, coherent backscattering, and damped quantum interference.[30] The localization length at the Dirac point of graphene is estimated to be ∼200 nm by two-dimensional scaling theory.[31] The predicted photocurrent may be suppressed to some extent by such effects.

We mention in passing that the effects of charge-transfer excitons, which are important for organic PV devices, have not been considered in our analysis because they are negligible for single-layer graphene, especially in the low photon energy regime (<1 eV).[32] Finally, we did not observe quantum interference between two electron paths accompanied by

resonant absorption of photons discussed theoretically in Ref. 33. The reason may lie in the mismatch of the device parameters that are required to satisfy both strong reflection and smooth potential profile. Hence to observe that phenomenon, we would need a device size on the order of 100 nm, which is much larger than the systems we investigated here.

To summarize, we have carried out a first-principles atomistic analysis of the photoresponse of graphene PN junctions. For both chemically doped and gate-controlled junctions, we examined several main features of the photoresponse function. Our calculations show that the graphene PN junctions have a broadband photoresponse—including terahertz, which is difficult to reach by conventional semiconductors. The dependence of photoresponse on the angle between the direction of light polarization and the PN interface is consistent with the previous theoretical prediction.[16] The overall trend of the dependence of photoresponse against photon energy, except for the chemical fingerprints observed in the chemically doped junctions, agrees well with that of the semiclassical model in the small intensity regime. Importantly, the essential properties of the photoresponse for the two kinds of PN junctions are found to be similar.

ACKNOWLEDGMENTS

We gratefully acknowledge financial support from NSERC of Canada, FQRNT of Quebec, and CIFAR. We thank RQCHP for providing computing facilities.

*chenj@physics.mcgill.ca

[1] F. Bonaccorso, Z. Sun, T. Hasan, and A. C. Ferrari, Nat. Photon. **4**, 611 (2010).
[2] A. B. Kuzmenko, E. van Heumen, F. Carbone, and D. van der Marel, Phys. Rev. Lett. **100**, 117401 (2008).
[3] C. H. Lui, K. F. Mak, J. Shan, and T. F. Heinz, Phys. Rev. Lett **105**, 127404 (2010).
[4] S.Bae *et al*., Nat. Nanotech. **5**, 574 (2010).
[5] P. Blake, P. D. Brimicombe, R. R. Nair, T. J. Booth, D. Jiang, F. Schedin, L. A. Ponomarenko, S. V. Morozov, H. F. Gleeson, E. W. Hill *et al*., Nano Lett. **8**, 1704 (2008).
[6] A. R. Wright, J. C. Cao, and C. Zhang, Phys. Rev. Lett. **103**, 207401 (2009).
[7] F. T. Vasko and V. Ryzhii, Phys. Rev. B **77**, 195433 (2008).
[8] A. Urich, K. Unterrainer, and T. Mueller, Nano Lett. **11**, 2804 (2011).
[9] T. Kampfrath, L. Perfetti, F. Schapper, C. Frischkorn, and M. Wolf, Phys. Rev. Lett. **95**, 187403 (2005).
[10] T. Mueller, F. Xia, and P. Avouris, Nat. Photon. **4**, 297 (2010).
[11] F. Xia *et al*., Nat. Nanotech. **4**, 839 (2009).
[12] A. V. Rozhkov, G. Giavaras, Y. P. Bliokh, V. Freilikher, and F. Nori, Phys. Rep. **503**, 77 (2011).
[13] J. Park, Y. H. Ahn, and C. Ruiz-Vargas, Nano Lett. **9**, 1742 (2009).
[14] F. Xia, T. Mueller, R. Golizadeh-Mojarad, M. Freitag, Y.-m. Lin, J. Tsang, V. Perebeinos, and P. Avouris, Nano Lett. **9**, 1039 (2009).
[15] E. C. Peters, E. J. H. Lee, M. Burghard, and K. Kern, Appl. Phys. Lett. **97**, 193102 (2010).
[16] S. Mai, S. V. Syzranov, and K. B. Efetov, Phys. Rev. B **83**, 033402 (2011).
[17] S. V. Syzranov, M. V. Fistul, and K. B. Efetov, Phys. Rev. B **78**, 045407 (2008).
[18] J. Taylor, H. Guo, and J. Wang, Phys. Rev. B **63**, 245407 (2001).
[19] J. Enkovaara, C. Rostgaard, J. J. Mortensen, J. Chen, M. Dułak, L. Ferrighi, J. Gavnholt, C. Glinsvad, V. Haikola, H. A. Hansen *et al*., J. Phys.: Condens. Matter **22**, 253202 (2010).
[20] X. Li, X. Wang, L. Zhang, S. Lee, and H. Dai, Science **319**, 1229 (2008).
[21] J. P. Perdew, K. Burke, and M. Ernzerhof, Phys. Rev. Lett. **77**, 3865 (1996).
[22] L. E. Henrickson, J. Appl. Phys. **91**, 6273 (2002).
[23] R. Lake and S. Datta, Phys. Rev. B **45**, 6670 (1992).
[24] See, for example, H. Haug and A.-P. Jauho, *Quantum Kinetics in Transport and Optics of Semiconductors* (Springer-Verlag, New York, 1998).
[25] M. Wu, C. Cao, and J.. Z. Jiang, Nanotechnology **21**, 505202 (2010).
[26] D. A. Stewart and F. Léonard, Phys. Rev. Lett. **93**, 107401 (2004).
[27] J. Taylor, H. Guo, and J. Wang, Phys. Rev. B **63**, 121104 (2001).
[28] In this work, we focused on the visible spectrum of solar light and we did not investigate the regime of photon energy $E_{\rm ph} > 3.0$ eV.
[29] In the numerical computation, a dense k-sampling is necessary to obtain smooth potential profiles; here 32 k-points along the x axis were used.
[30] E. McCann, K. Kechedzhi, V. I. Fal'ko, H. Suzuura, T. Ando, and B. L. Altshuler, Phys. Rev. Lett. **97**, 146805 (2006).
[31] A. Lherbier, X. Blase, Y.-M. Niquet, F. Triozon, and S. Roche, Phys. Rev. Lett. **101**, 036808 (2008).
[32] L. Yang, J. Deslippe, C.-H. Park, M. L. Cohen, and S. G. Louie, Phys. Rev. Lett. **103**, 186802 (2009).
[33] M. V. Fistul, S. V. Syzranov, A. M. Kadigrobov, and K. B. Efetov, Phys. Rev. B **82**, 121409 (2010).